SCIENCE CHINA
Information Sciences

• RESEARCH PAPER •

April 2016, Vol. 59 042413:1–042413:9
doi: 10.1007/s11432-016-5529-5

Investigation of plasmonic whispering gallery modes of graphene equilateral triangle nanocavities

Yixin HUANG[1], Weibin QIU[1]*, Shangxin LIN[1], Jing ZHAO[1], Houbo CHEN[1], Jia-Xian WANG[1], Qiang KAN[2] & Jiao-Qing PAN[2]

[1]*College of Information Science and Engineering, Huaqiao University, Xiamen* 361021*, China;*
[2]*Institute of Semiconductors, Chinese Academy of Sciences, Beijing* 100083*, China*

Received August 3, 2015; accepted October 20, 2015; published online February 17, 2016

Abstract In this paper, a graphene-based equilateral triangle nanocavity is proposed and numerically investigated. The relationship between the mode characteristics and the nanocavity parameters, such as the geometry of nanocavity and the chemical potential of graphene, is systematically explored. A high-order plasmonic WGM (whispering gallery mode) with a high quality factor of 147.93 is obtained in our nanocavity with a wavelength of around 1.415 μm in free space, with a corresponding Purcell factor as high as 7.067×10^8. The proposed plasmonic WGM nanocavity could be a key component of the high density plasmonic integrated circuits due to its ultra-compactness and performances.

Keywords graphene, nanocavity resonator, surface plasmonic polaritons, whispering gallery mode, plasmonic integrated circuits

Citation Huang Y X, Qiu W B, Lin S X, et al. Investigation of plasmonic whispering gallery modes of graphene equilateral triangle nanocavities. Sci China Inf Sci, 2016, 59(4): 042413, doi: 10.1007/s11432-016-5529-5

1 Introduction

Whispering-gallery-mode (WGM) microcavities with an extremely small mode volume (V_{m}) and a high quality factor (Q factor) are favorable structures of the low-threshold lasers and filters. However, the sizes of the conventional dielectric WGM microcavities are usually in a wavelength level [1]. Further miniaturization of the microcavities is challenging due to the diffraction limit, which prevents the microresonators from wide applications in high density photonic integrated circuits. On the other hand, surface plasmon polaritons (SPPs) which exist in the interface between metal and dielectric, could concentrate and guide the electromagnetic (EM) field in a deep subwavelength scale [2]. Hence, the dimensions of the metal-coated WGM microcavities which combine the advantages of surface plasmon polaritons and whispering gallery modes, could be reduced to far beyond the diffraction limit. Generally, the noble metals are employed as the plasmonic materials [3, 4]. Although the metal-coated WGM microcavities have solved the problem about the miniaturization of the cavities, another problem of the large ohmic loss arises in this class of microcavities. The ohmic loss severely deteriorates the Q factor of the cavities and eventually degrades the optical performance. In addition, it is difficult to tune the plasmons once the

* Corresponding author (email: wbqiu@hqu.edu.cn)

device geometry is determined. Accordingly, other plasmonic materials with more outstanding material properties are highly desired.

Graphene, a one-atom-thick material with a honeycomb lattice, has been widely studied [5,6] due to its unique plasmonic properties. Compared with the noble metals, graphene offers the advantages including a higher confinement ability of EM field and a relatively longer propagation length [7]. Futhermore, the graphene supported plasmon is tunable, which is impossible in the counterpart supported by the noble metals. Therefore, the graphene-based plasmonic WGM microcavities are regarded as an appropriate substitute for the metal-coated plamonic WGM microcavities. According to Kubo's formula [7,8], graphene's conductivity σ_{g} is composed of the contributions from both the interband electron transitions σ_{inter}, and the intraband electron-photon scattering σ_{intra}, i.e. $\sigma_{\mathrm{g}} = \sigma_{\mathrm{inter}} + \sigma_{\mathrm{intra}}$. In more detail,

$$\sigma_{\mathrm{inter}} = \mathrm{i}\frac{e^2}{4\pi\hbar}\ln\left[\frac{2|\mu_{\mathrm{c}}| - \hbar(\omega + \mathrm{i}\tau^{-1})}{2|\mu_{\mathrm{c}}| + \hbar(\omega + \mathrm{i}\tau^{-1})}\right], \tag{1}$$

$$\sigma_{\mathrm{intra}} = \mathrm{i}\frac{e^2\mathrm{k_B T}}{\pi\hbar^2(\omega + \mathrm{i}\tau^{-1})}\left[\frac{\mu_c}{\mathrm{k_B T}} + 2\ln\left(\exp\left(-\frac{\mu_{\mathrm{c}}}{\mathrm{k_B T}}\right) + 1\right)\right], \tag{2}$$

where μ_c is the chemical potential, ω is the angular frequency of the plasmon, and τ is the electron momentum relaxation time. Specifically, the chemical potential of graphene could be tuned conveniently by means of the electrostatic gating or the chemical doping [9]. Recent experimental work shows that a chemical potential as high as 2 eV was achieved [10]. Also, a relaxation time as high as 3 ps was reported experimentally [11]. In this work, we assume that the relaxation time is less than 1.5 ps, and the chemical potential is lower than 1 eV. Such low relaxation time and chemical potential are conservative enough to ensure the reliability of our numerical study.

In the past years, there has been obvious progress in the investigation of the circular structure of WGM microcavities such as microdisks and cylinder cavities [12,13]. However, the directional emission which is obtained from the single perfect circular cavity is greatly limited owing to the perfect symmetry property and the nearly total internal reflection at the lateral boundary of the cavity [14]. Various polygonal microcavity structures such as hexagon [15], rectangular [16,17], square [18–21] and triangle [22–24] have demonstrated the excellent performances. The previous research shows that the equilateral triangle resonant microcavities are suitable to realize the single-mode and directional emission operation [25], which is particularly important to the tehnique of the PIC (photonic integrated circuits) or on-chip photonic interconnect technique. Actually, the absorption spectra and the absorption cross-section spectra of perfect arm-chair edge triangle graphene nano structures have been calculated based on quantum mechanics [26]. However, they only demonstrate the resonance peak positions and the relative intensity of the peak. The detailed EM field distribution, as well as the characteristic parameters such as mode volume, Q factor, and their dependence on the geometry and the material properties still remain unclear. Furthermore, the physical mechanisms behind these relations are yet unknown.

In this article, we propose a graphene nanoresonator formed by an equilateral triangular graphene section with a chemical potential μ_{c1} which is surrounded by the rest of the same piece of infinite graphene sheets with the chemical potential μ_{c2}. According to Kubo's formula, the surface conductivity of the graphene sheet is determined by the chemical potential. The chemical potential here is analogical with the refractive index of the dielectric materials, but it is tunable by either electric gate or local chemical doping. The EM field distribution, the mode volume, quality factor, and their dependence on the geometry and the material properties are explored systematically. Also, the physical mechanisms behind these dependent relations are revealed. The proposed structure can be a fundamental structure of the directional emitters or filters in the future plasmonic integrated circuit or on-chip plasmonic inter-connect technique. The rules revealed in this article provide an effective route to optimize the structures of the nanoresonators.

2 Model in numerical study

The schematic diagram of this tunable graphene-based nanocavity is shown in Figure 1, where R_1 and R_2 represent the radius of the circumscribed circle of the equilateral triangular section and the cavity

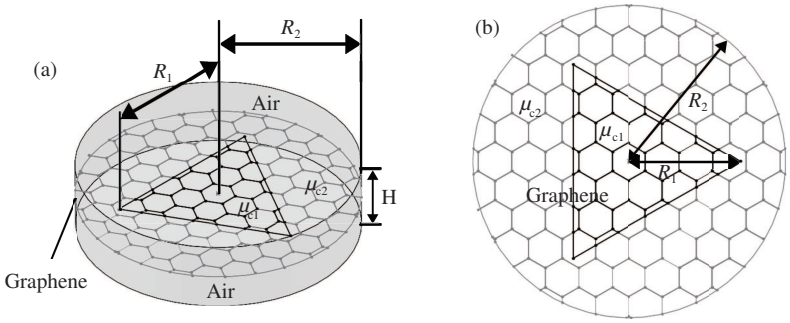

Figure 1 The schematic diagram of the graphene-based equilateral triangle nanocavity. (a) 3-dimensional view; (b) cross-sectional view. The cavity is composed of a single sheet of infinite freestanding graphene which has an equilateral triangular section with a chemical potential, which differs from the other section of the same graphene. Here, μ_{c1} and μ_{c2} indicate different chemical potentials. R_1 and R_2 represent the radius of the circumscribed circle of the equilateral triangle and the cavity outer radius, respectively. The regions which are above and below the graphene represent the air layers with the height of H, which are the computational windows for our numerical simulation.

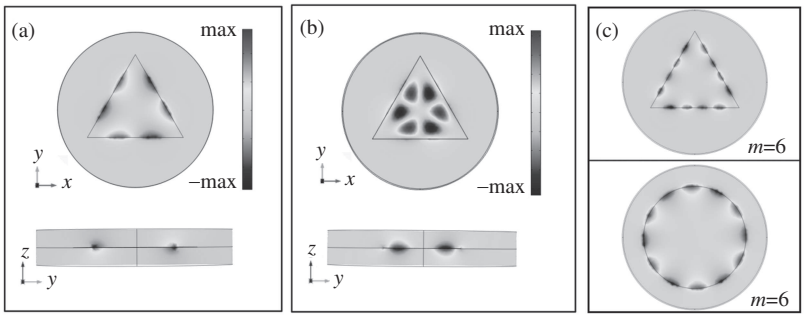

Figure 2 The cross-sectional and vertical profile of the electric field z component E_z with $\mu_{c1} = 0.9$ eV and $\mu_{c2} = 0.5$ eV at the resonance frequency of (a) 212 THz and (b) 216 THz. (a) Fundamental mode TM_{31} with the azimuthal mode number of 3 and the radial mode number of 1. (b) High-order mode TM_{32} with the azimuthal mode number of 3 and the radial mode number of 2. For comparison, the electric field z component distribution of the fundamental modes in the equilateral triangle nanocavity and the circular nanocavity are shown in (c), where the azimuthal mode number is 6. Here, the radius $R_1 = 10$ nm, $R_2 = 14$ nm and the relaxation time $\tau = 0.5$ ps.

outer radius of the computational window, respectively. Here, the gray regions which are above and below the graphene are the air layers. We numerically study the plasmonic WGM characteristics of this graphene-based equilateral triangle nanoresonator by using the eigenfrequency solver of the commercial software COMSOL Multiphysics, Version 4.3b, RF Module. It should be pointed out that the thickness of the graphene monolayer is far below the wavelength of the light wave [8,27]. So it is treated as a zero-thickness [27] layer with the surface conductivity σ_g in our numerical investigation. The graphene sheet is characterized by $J = \sigma_g E$ [7], where J is the surface current density and E is the electric componenet of the EM field of the plasmons.

As shown in Figure 2(a), a fundamental mode with an azimuthal mode number of 3, i.e. TM_{31}, is obtained in the graphene-based equilateral triangle nanocavity, where the resonance wavelength in free space is 1.42 μm. Another mode shown in Figure 2(b) is a high-order plasmonic WGM with an azimuthal mode number of 3 and a radial mode number of 2, i.e. TM_{32}, at a resonance wavelength of 1.39 μm in free space. The two modes are obtained under the conditions that $\mu_{c1} = 0.9$ eV, $\mu_{c2} = 0.5$ eV, $R_1 = 10$ nm and $R_2 = 14$ nm. The vertical distribution profiles of the two modes in Figure 2 show that the electric field of the EM field is tightly confined by graphene, verifying the superior light confinement property of graphene. Of course, due to different phases, the mode field distribution could also exist in the vertex. As is shown in Figure 2(c), the mode field distribution in the vertexes of the triangle is weak, and the high Q factor modes could be maintained as an output waveguide, which is directly connected to the vertex of the triangular nanocavity [28]. Hence the waveguide connected equilateral triangle nanocavity easily realizes the directional emission of the high Q modes. However, the weak field points distribution

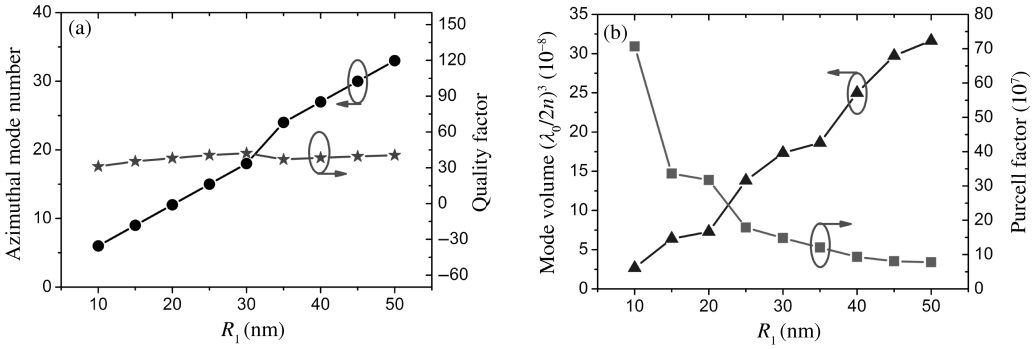

Figure 3 (a) The dependence of the azimuthal mode number and the quality factor on R_1; (b) the effective mode volume and the Purcell factor of the equilateral triangle nanocavity are calculated as a function of the geometry parameter R_1. Here, $\mu_{c1} = 0.9$ eV and $\mu_{c2} = 0.5$ eV. In addition, the relaxation time of the graphene is kept in 0.5 ps and the resonance frequency is set as 220 THz approximately.

in the circumference of circular nanocavity is homogeneous, and it is difficult to be determined during the design. Therefore, the Q factor of the circular nanocavity connected with a waveguide is expected to have a serious reduction, except some coupled modes induced by the destroyed circular symmetry [28]. In addition, the equilateral triangular nanocavity has fewer modes than the circular nanocavity with similar areas [29], and the high order modes have a relatively high Q factor than the fundamental modes, which is more natural to reach single mode operation.

The light-matter interaction can be represented by mode volume ($V_{\rm m}$) and quality factor (Q factor) [30]. The effective mode volume is expressed by

$$V_{\rm m} = \frac{\int W(\boldsymbol{r}){\rm d}^3\boldsymbol{r}}{\max[W(\boldsymbol{r})]}. \tag{3}$$

Here, the electromagnetic energy density $W(\boldsymbol{r})$ is given by $W(\boldsymbol{r}) = \frac{1}{2}[\frac{1}{\mu_0}|B(\boldsymbol{r})|^2 + \frac{{\rm d}(\epsilon(\boldsymbol{r})\omega)}{{\rm d}\omega}|E(\boldsymbol{r})|^2]$ [31] where $B(\boldsymbol{r})$ and $E(\boldsymbol{r})$ are the magnetic field and the electric field, $\max[W(\boldsymbol{r})]$ is the maximal electromagnetic energy density, respectively. The integral is taken in the whole space. In general, a smaller mode volume suggests stronger electromagtic field localization, which eventually results in stronger light-matter interaction. The other key parameter of the resonators is Q factor. For a resonator, a higher Q factor indicates a longer life span of photon, and further suggests stronger light-matter interaction. The radiation loss and absorption loss, which are regarded independent from each other, are two main loss sources in the cavities. Therefore, we divide the total Q factors of the nanocavity into $Q_{\rm rad}$ which relates to the radiation losses, and $Q_{\rm abs}$ which relates to the absorption losses [30], i.e., $Q_{\rm total}^{-1} = Q_{\rm rad}^{-1} + Q_{\rm abs}^{-1}$. In addition, the $Q_{\rm abs}$ is calculated by

$$Q_{\rm abs} = \frac{|r(\beta)|}{2 \times |i(\beta)|}, \tag{4}$$

where $r(\beta)$ and $i(\beta)$ are the real part and the imaginary part of the propagation constant β of the SPPs mode, respectively. The real part of the propagation constant $r(\beta)$ can be expressed as $k_0 n_{\rm eff}$. Here, $n_{\rm eff}$ represents the SPPs effective mode index indicating the confinement ability of graphene, while the imaginary part of the propagation constant indicates the losses of SPPs.

3 The effect of cavity sizes on mode characteristics

In order to understand the influence of the size of the nanocavity on the mode characteristics, we first explore the Q factor and the effective mode volume at different R_1 of the graphene equilateral triangle nanocavity when the resonance frequency is kept at 220 THz. The chemical potentials of different regions are set as $\mu_{c1} = 0.9$ eV and $\mu_{c2} = 0.5$ eV, respectively. Figure 3(a) plots the azimuthal number and Q factor as a function of R_1. The Q factor is always around 45 when R_1 increases from 10 nm to 50 nm, while the azimuthal mode number keeps increasing monotonously. The propagation length of the SPPs

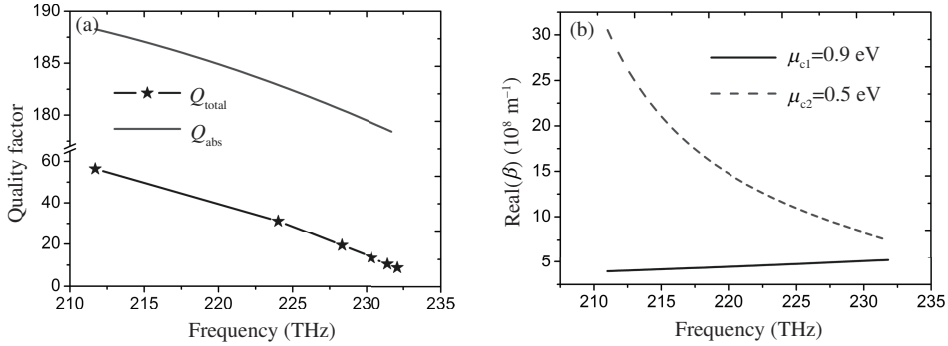

Figure 4 (a) Quality factor (star symbols) of SPPs guided WGM obtained from the numerical simulation and absorption-loss-limited Q factor $Q_{\rm abs}$ (solid line) calculated from Eq. (4) as a function of the resonance frequency. And the data points (star symbols) correspond to different modes, each of which has different resonant frequency. Here, $\mu_{\rm c1} = 0.9$ eV and $\mu_{\rm c2} = 0.5$ eV. For comparison, R_1 is kept at 10 nm. The relaxation time is 0.5 ps. (b) The real part of the propagation constant as a function of frequency along a single freestanding graphene sheet, when the chemical potentials are 0.9 eV (solid line) and 0.5 eV (dash line).

wave gradually decreases with the diminution of R_1, which results in the reduction of absorption losses. Therefore, the $Q_{\rm abs}$ increases. In the meantime, $Q_{\rm rad}$ shifts down due to the augment of the radiation loss, which is rooted in the lower confinement capability of a smaller curvature radius of the circumscribed circle [32]. As mentioned above, the Q factor of the resonant cavity is mainly limited by the radiation loss and the absorption loss. The overall effect of these mechanisms explains the trivial variation of the total Q factor in our equilateral triangle nanocavity. Besides, Figure 3(b) shows that when the R_1 shifts down, the effictive mode volume decreases monotonously, indicating the stronger spatial confinement of the EM field. The Purcell factor [32] that relates to spontaneous emission is obtained by

$$F = \frac{3}{4\pi^2}\left(\frac{\lambda_0}{n}\right)^3 \frac{Q}{V_{\rm m}}. \tag{5}$$

The effective mode volume ($V_{\rm m}$) and quality factor (Q factor) are obtained from Figure 3(a) and (b), and the relation between the Purcell factor and R_1 is calculated following Eq. (5), which is also plotted in Figure 3(b). The corresponding Purcell factor grows up monotonously with the reduction of R_1, and reaches 7.067×10^8 at $R_1 = 10$ nm.

4 The dependence of mode characteristics on graphene's surface conductivity

Besides the geometry parameters of the nanocavity, the characteristic parameters of graphene, such as chemical potential, relaxation time, and also, the resonant frequency, has significant effects on the graphene's surface conductivity. In order to understand the role of these parameters, we further study the Q factor and mode volume under different conditions.

4.1 The Q factor and mode volume of the plasmonic WGM at different frequency

First, we explore the plasmonic WGM properties of the graphene-based equilateral triangle nanocavity at different resonance frequency when $R_1 = 10$ nm, $\mu_{\rm c1} = 0.9$ eV, $\mu_{\rm c2} = 0.5$ eV and $\tau = 0.5$ ps. It is shown in Figure 4(a) that the total Q factor reduces monotonically from 56.4 to 9.2 along with the increase of the resonance frequency from 211 THz to 232 THz. Meanwhile, the absorption loss-limited Q factor $Q_{\rm abs}$ calculated by Eq. (4) decreases from 188.2 to 178.4, shown in Figure 4(a). $Q_{\rm abs}$ is higher than the total quality factor of the nanocavity. Therefore, the decrease of Q factor is not only attributed to the absorption loss, but also limited by the radiation loss. On the one hand, the absorption loss increases with the frequency, leading to a reduction of $Q_{\rm abs}$ shown in Figure 4(a). On the other hand, the dispersion relation of the plasmons propagating along the infinite freestanding graphene sheets with uniform chemical potentials of 0.9 eV and 0.5 eV is shown in Figure 4(b). As the frequency increases from

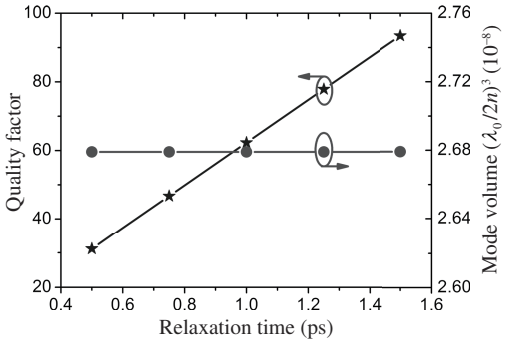

Figure 5 The quality factor and the efficient mode volume versus the relaxation time of the graphene. The size of the cavity is kept as $R_1 = 10$ nm. For comparison, the chemical potential and the resonance frequency are kept at $\mu_{c1} = 0.9$ eV, $\mu_{c2} = 0.5$ eV and 220 THz.

210 to 232 THz, the propagation constants of the two chemical potentials become closer, which means that the momentum $\hbar\mathrm{Re}(\beta)$ of the two plasmons becomes more matched. Therefore the plasmon tends to escape from the nanocavity which would result in a lager radiation loss, and Q_{rad} degrades accordingly [4]. As a result, the total quality factor shifts down obviously under these factors. In addition, the mode volume of this nanocavity is smaller than $10^{-8}(\lambda_0/2n)^3$ at a frequency of 232 THz, which indicates a strong light-matter interaction.

4.2 The Q factor and mode volume of the plasmonic WGM at different relaxation time of the graphene

Next, the effective mode volume and the quality factor of the plasmonic WGM, which depend on the relaxation time of the graphene at the resonant frequency of 220 THz, are plotted in Figure 5, where the chemical potential μ_{c1} and μ_{c2} are set as 0.9 eV and 0.5 eV, respectively. The circumscribed circle's radius of the nanocavity R_1 is kept at 10 nm for comparision. The plasmonic WGM behaviors in Figure 5 show that the mode volume remains at approximately $2.68 \times 10^{-8}(\lambda_0/2n)^3$ when the relaxation time increases from 0.5 ps to 1.5 ps. Meanwhile, the Q factor linearly increases from 31.1 to 93.4. The increase of the relaxation time of graphene, which is inversely proportional to the charge particle scattering rate Γ [33,34], leads to the decrease of absorption losses. This eventually results in the rise of the Q factor. Thus, the relaxation time is the main factor that governs the Q factor of a given graphene nanoresonator. However, the EM field confinement capability of the equilateral triangle nanocavity has not been improved.

4.3 The Q factor and mode volume of the plasmonic WGM at different chemical potentials of the graphene

We study the relation between the Q factor and the azimuthal mode number with the chemical potentials of μ_{c1} and μ_{c2}, respectively. For the fundamental modes at a frequency of 220 THz shown in Figure 6(a), it is obvious that the quality factor rapidly rises and then slightly decreases when the chemical potential μ_{c1} increases from 0.75 eV to 1.10 eV. The maximum value reaches 56.4 at $\mu_{c1} = 0.9$ eV. Considering the influence of the chemical potential of the rest area μ_{c2}, one can see from Figure 6(b) that the Q factor exhibits a slight decrease when the chemical potential μ_{c2} shifts down from 0.54 eV to 0.50 eV, and then sharply falls down to less than 10 when the chemical potential μ_{c2} further decreases. It should be noted that the azimuthal mode number decreases with the increase of the chemical potential until it falls down to 3.

Last, we investigate the effect of the chemical potential μ_{c2} on the Q factor of the higher order plasmonic WGMs in the proposed nanocavity. The size of the equilaterial triangle nanocavity with R_1 of 30 nm and the chemical potential μ_{c1} of 0.9 eV are set. The insets in Figure 7 show the distribution of electric field z component E_z of TM_{32} and TM_{33}, respectively. Here, the corresponding resonant frequencies of these two high-order modes are around 212 THz and 234 THz. The Q factor of TM_{32} and TM_{33} are calculated at different chemical potentials μ_{c2}, as shown in Figure 7. The Q factor of TM_{32} slowly increases when

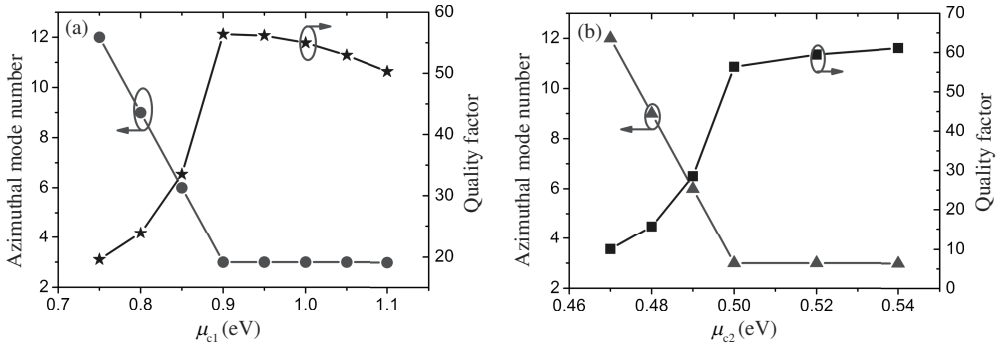

Figure 6 The azimuthal mode number and Q factor as a function of the chemical potential. (a) The azimuthal mode number and the Q factor as a function of the chemical potential μ_{c1}. Another chemical potential μ_{c2} is fixed at 0.5 eV. (b) The dependence of the azimuthal mode number and the Q factor on the chemical potential μ_{c2}. The chemical potential μ_{c1} remains a constant of 0.9 eV, and the resonant wavelength is set around 1.36 μm.

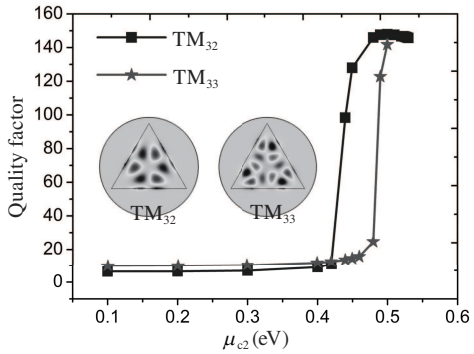

Figure 7 The Q factor of the high-order modes TM_{32} (square symbols) and TM_{33} (star symbols) as a function of the chemical potential μ_{c2}. Here, the chemical potentials of equilateral triangular section μ_{c1} and the relaxation time of the graphene are fixed at 0.9 eV and 0.5 ps, respectively.

μ_{c2} varies from 0.1 eV to 0.42 eV, but it is less than 20. As μ_{c2} further increases, the Q factor of TM_{32} rapidly rises until it reaches the maximum value of 147.9 at μ_{c2} of 0.5 eV, and then it declines slightly. Moreover, the Q factor of TM_{33}, which is slightly different from that of TM_{32} at the beginning, starts to rapidly increase to greater than 20 only when μ_{c2} reaches 0.46 eV. It is well known that as the chemical potential gradually approaches $\hbar\omega/2$, the real part of the surface conductivity is gradually dominated by the interband transition, which would induce the increase of the loss or even finally the disappearance of SPPs [7]. For a certain frequency of 212 THz in this section, the $\hbar\omega/2$ is around 0.43 eV. As is shown in Figure 7, when the μ_{c2} decreases from 0.5 eV to 0.42 eV, the Q factor of TM_{32} deteriorates severely, which is in conformity with the variation tendency of the interband transition. However, one can see that the mode field distribution mainly concentrates on the graphene nanocavity, the chemical potential of which μ_{c1} is a constant. The dominated interband transition in the surface conductivity of the large area of graphene could result in losses, but it is not the main reason for the huge reduction of the Q factor. In addition, the variation of the Q factor cannot be explained by the interband transition in the section where the chemical potential changes from 0.56 eV to 0.50 eV or 0.42 eV to 0.1 eV. The similar result also occurs in the TM_{33} mode. To understand this behavior, we model a graphene nanoribbon waveguide structure in Figure 8(a). The waveguide is composed of a graphene nanoribbon of the width R_1 with a chemical potential of μ_{c1} sandwiched by a larger area of graphene with variable chemical potentials of μ_{c2}. The real and imaginary parts of the propagration mode index are plotted in Figure 8(b) and Figure 8(c) as a function of μ_{c2}. In Figure 8(b) where the frequency is 212 THz, the imaginary part of the effective mode index n_{eff} decreases monotonously, but the variation is not obvious when the μ_{c2} increases from 0.1 eV to 0.42 eV, which indicates that the absorption loss of SPPs only shifts down slightly. Meanwhile, the radiation loss is also large due to the relatively small real part of n_{eff}. Hence, the total Q factor of

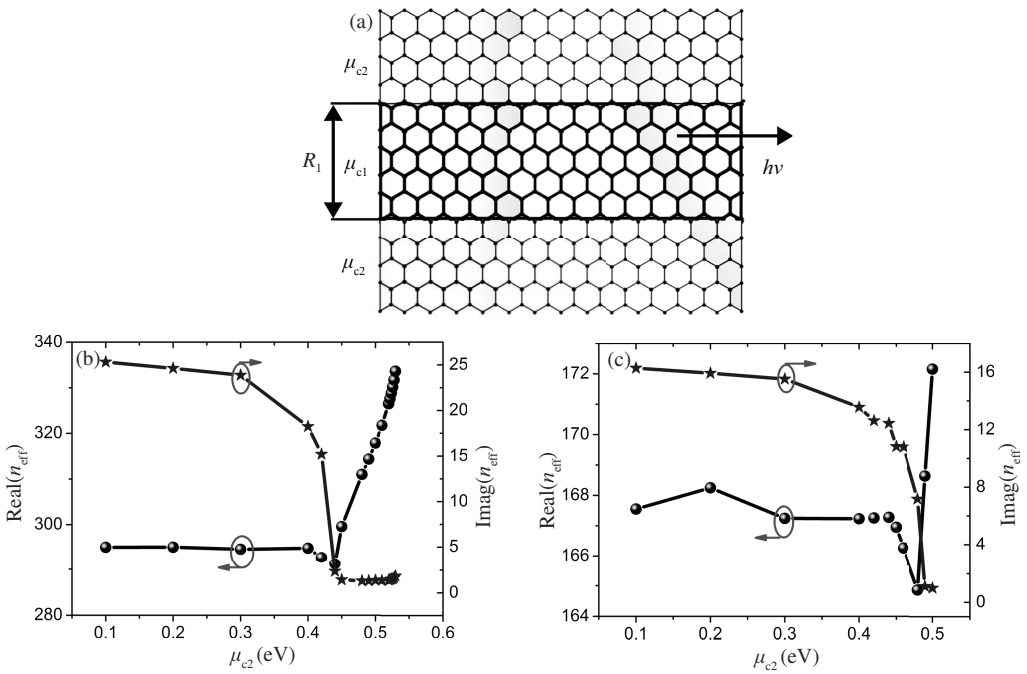

Figure 8 (a) The schematic diagram of the graphene nanoribbon waveguide structure which consists of a nano scale ribbon-like section with the chemical potential μ_{c1} which is surrounded by the other two sections on the same sheet of graphene, but with a different chemical potential μ_{c2}. The real part (sphere symbols) and the imaginary part (star symbols) of the effective SPPs index at different chemical potentials μ_{c2} of the graphene area sandwich the nanoribbon-like section when the frequency is set as (b) 212 THz and (c) 234 THz.

TM_{32} is quite low in this region. Then, the imaginary part rapidly decreases and obtains its minimum value at 0.5 eV, which is an evidence for the rapid increase of the Q factor of TM_{32}. In the region where the chemical potential μ_{c2} varies from 0.50 eV to 0.53 eV, the imaginary part of effective mode index increases slightly, and the real part is also large enough. As a result of these mechanisms, the Q factor only increases slightly. Obviously, the imaginary part of n_{eff} sharply decreases as μ_{c2} becomes larger than 0.48 eV in Figure 8(c), similar to TM_{32}, which can explain the behavior of the Q factor of TM_{33}.

Practically, graphene may be supported by a substrate rather than being isolated in free space. In this case, the EM field distribution and the rules of the parameters are still valid though the substrate can introduce quantitative differences. To fabricate the real structures, one can follow the approaches proposed by Vakil and Engheta [9], where the nanoresonator with a radius of 10 nm can be formed by (1) the appropriate design of the electric gate, (2) the uneven ground plane, and (3) the inhomogeneous distribution of the permittivity. The 10 nm scale patterns can be defined by the electron-beam lithography or the focused ion beam (FIB) technique, or by the self-assemble material growth method.

5 Conclusion

In conclusion, we have proposed a graphene-based equilateral triangular nanocavity with a size of tens of nanometers. The plasmonic WGM properties including the mode volume and Q factors have been numerically predicted as a function of the parameters of the triangle nanoresonators in the near infrared region. The proposed surface-plasmonic whispering-gallery nanocavity could be one of the key components for a wide range of nanophotonic devices such as the single photon source, the subwavelength single photon transistor, or the low threshold emission sources. Furthermore, it could be a major component of the high-density plasmonic integrated circuit or on-chip plasmonic interconnect technique in the future.

Acknowledgements The work was supported by National Natural Science Foundation of China (Grant No. 61378058), Science and Technology Fund of Quanzhou (Grant No. Z1424009), and Opened Fund of the Key

Laboratory on Semiconductor Materials (Grant No. KLSMS-1201)

Conflict of interest The authors declare that they have no conflict of interest.

References

1 Gramotnev D K, Bozhevolnyi S I. Plasmonics beyond the diffraction limit. Nat Photonics, 2010, 4: 83–91
2 Barnes W L, Dereux A, Ebbesen T W. Surface plasmon subwavelength optics. Nature, 2003, 424: 824–830
3 Kim M W, Chen Y, Moore J, et al. Subwavelength surface plasmon optical cavity-scaling, amplification, and coherence. IEEE J Sel Top Quant, 2009, 15: 1521–1528
4 Chen Y L, Zou C L, Hu Y W, et al. High-Q plasmonic and dielectric modes in a metal-coated whispering-gallery microcavity. Phys Rev A, 2013, 87: 023824
5 Mikhailov S A, Ziegler K. New electromagnetic mode in graphene. Phys Rev Lett, 2007, 99: 016803
6 Ju L, Geng B, Horng J, et al. Graphene plasmonics for tunable terahertz metamaterials. Nat Nanotechnol, 2011, 6: 630–634
7 Zhao J, Qiu W, Huang Y, et al. Investigation of plasmonic whispering-gallery mode characteristics for graphene monolayer coated dielectric nanodisks. Opt Lett, 2014, 39: 5527–5530
8 Hanson G W. Dyadic green's functions and guided surface waves for a surface conductivity model of graphene. J Appl Phys, 2008, 103: 064302
9 Vakil A, Engheta N. Transformation optics using graphene. Science, 2011, 332: 1291–1294
10 Efetov D K, Kim P. Controlling electron-phonon interactions in graphene at ultra high carrier densities. Phys Rev Lett, 2010, 105: 256805
11 Low T, Avouris P. Graphene plasmonics for terahertz to mid-infrared applications. ACS Nano, 2014, 8: 1086–1101
12 Yang Y D, Huang Y Z, Guo W H, et al. Enhancement of quality factor for TE whispering-gallery modes in microcylinder resonators. Opt Express, 2010, 18: 13057–13062
13 Chen Y H, Guo L J. Analysis of surface plasmon guided sub-wavelength microdisk cavity. In: Proceedings of LEOS the 21st Annual Meeting of the IEEE Lasers and Electro-Optics Society, Acapulco, 2008. 320–321
14 Chen Q, Hu Y H, Huang Y Z, et al. Equilateral-triangle-resonator injection lasers with directional emission. IEEE J Quantum Elect, 2007, 43: 440–444
15 Lin J D, Huang Y Z, Yang Y D, et al. Single transverse whispering-gallery mode AlGaInAs/InP hexagonal resonator microlasers. IEEE Photonics J, 2011, 3: 756–764
16 Wang S J, Huang Y Z, Yang Y D, et al. Long rectangle resonator 1550 Nm AlGaInAs/InP lasers. J Opt Soc Am B, 2010, 27: 719–724
17 Yang Y D, Huang Y Z. Mode analysis and Q-factor enhancement due to mode coupling in rectangular resonators. IEEE J Quantum Elect, 2007, 43: 497–502
18 Chen Q, Huang Y Z, Guo W H, et al. Analysis of modes in a freestanding microsquare resonator by 3-D finite-difference time-domain simulation. IEEE J Quantum Elect, 2005, 41: 997–1001
19 Huang Y Z, Chen Q, Guo W H, et al. Experimental observation of resonant modes in GaInAsP microsquare resonators. IEEE Photonic Tech L, 2005, 17: 2589–2591
20 Che K J, Huang Y Z. Mode characteristics of metallically coated square microcavity connected with an output waveguide. J Appl Phys, 2010, 107: 113103
21 Che K J, Yang Y D, Huang Y Z. Multimode resonances in metallically confined square-resonator microlasers. Appl Phys Lett, 2010, 96: 051104
22 Huang Y Z, Chen Q, Guo W H, et al. Mode characteristics for equilateral triangle optical resonators. IEEE J Sel Top Quant, 2006, 12: 59–65
23 Yang Y D, Huang Y Z. Symmetry analysis and numerical simulation of mode characteristics for equilateral-polygonal optical microresonators. Phys Rev A, 2007, 76: 023822
24 Wysin G M. Electromagnetic modes in dielectric equilateral triangle resonators. J Optical Soc Am B, 2006, 23: 1586–1599
25 Huang Y Z, Guo W H, Yu L J, et al. Analysis of semiconductor microlasers with an equilateral triangle resonator by rate equations. IEEE J Quantum Elect, 2001, 37: 1259–1264
26 Garcia de Abajo F J. Graphene plasmonics: challenges and opportunities. ACS Photonics, 2014, 1: 135–152
27 Qiu W, Liu X, Zhao J, et al. Nanofocusing of mid-infrared electromagnetic waves on graphene monolayer. Appl Phys Lett, 2014, 104: 041109
28 Yang Y D, Wang S J, Huang Y Z. Investigation of mode coupling in a microdisk resonator for realizing directional emission. Opt Express, 2009, 17: 23010–23015
29 Liu D, Hattori H T, Fu L, et al. Single-mode operation of a large optically pumped triangular laser with lateral air trenches. J Opt Soc Am B, 2009, 26: 1417–1422
30 Kwon S H. Deep subwavelength plasmonic whispering-gallery-mode cavity. Opt Express, 2012, 20: 24918–24924
31 Xiao Y F, Li B B, Jiang X, et al. High quality factor, small mode volume, ring-type plasmonic microresonator on a silver chip. J Phys B-At Mol Opt, 2010, 43: 035402
32 Vahala K J. Optical microcavities. Nature, 2003, 424: 839–846
33 Gosciniak J, Tan D T H. Theoretical investigation of graphene-based photonic modulators. Sci Rep-UK, 2013, 3: 01897
34 Chen P Y, Alù A. Atomically thin surface cloak using graphene monolayers. ACS Nano, 2011, 5: 5855–5863